Magnetospheric Coherent Structures in 3D Global MHD Simulations Focusing on Alfvenic Kármán Vortex Dynamics

D. Cai[1], Y. Jiang[1], B. Lembège[2], Y. Kubota[3], and S. Fujita[4]

[1]University of Tsukuba, Tsukuba, Japan, cai@cs.tsukuba.ac.jp, [2]LATMOS - UVSQ - CNRS, Guyancourt, France, [3]NICT, Koganei, Tokyo, Japan, [4]Meteorological College, Kashiwa, Japan

Abstract

Magnetospheric coherent structures related to the dynamics of the dayside magnetopause frontier for a northward IMF configuration, are analyzed using global 3D MHD simulations. The main goal is to reach a synthetic scenario on the formation of 3D unstable/stable structures developed in different steps from the dayside to the night side. They are: (i) the transverse Kelvin-Helmholtz (K-H) vortexes are generated along and outside the magnetopause near the dayside region, while other K-H vortexes are generated along and inside the magnetopause; (ii) both rows of vortexes are shed off soon from the magnetopause; (iii) these vortexes are unstable in one each row, adjust, and evolve into a marginal stable Kármán vortex street; (iv) these Kármán vortexes soon are reformed into stable longitudinal (stream-wise) coherent vortexes and survive for long time over large distances x~-130 to 140Re in the magnetotail. All these processes lead to the formation of magnetospheric coherent structures.

Keywords: Alfvenic vortex shedding, Kármán vortex Street, Strouhal Number, Kelvin-Helmholtz instability, and Vortex core line

Key Points: Along the two sides of magnetopause, the solar wind and magnetospheric flows generate Alfvenic Kármán vortex streets. A regular Alfvenic Karman vortex shedding and its outcome as a vortex street are observed in the 3D global MHD simulation. The Karman vortex shedding is useful for understanding the origin of magnetospheric coherent structure.

1, Introduction

The Kelvin-Helmholtz instability (referred to as K-H throughout the paper), is

a linear shear instability and can occur in a fluid or a plasma flow where a velocity shear is generated in a single continuous fluid or plasma, or where a velocity difference is generated across two fluids or plasmas [*Chandrasekhar*, 1968]. The K-H instability can generate linear "transverse" vortexes whose core lines are almost perpendicular to the shear flows as illustrated in Fig. 1(a). These linear transverse vortexes grow inside the shear layers, and soon the growths of linearly unstable modes saturate, the vortexes shed-off from the shear layers, and become the so-called free vortexes. Recently, several papers have discussed the Kelvin-Helmholtz (K-H) instability and its related waves and vortex structures by using global 2D/3D MHD simulations[*Guo et al.*, 2010; *Li et al.*, 2012; *Li et al.*, 2013; *Merkin et al.*, 2013]. Merkin et al.(2013) found a double-vortex sheet in which a vortex train propagates along the inner and outer edges of the magnetopause as shown in Fig. 1(b). Two vortex sheets composed with paired vortices rotating in opposite direction one each other are formed as displayed in Fig. 2 (a). In the figure, vortexes flow from left to right and align in two rows of opposite rotation one to each other in a staggered manner with the aspect ratio R=a/b~0.281. This structure suggests a double vortex sheet of velocity perturbations and is most apparent behind the dawn-dusk "terminator" (i.e., x=0 in Figure 1(b), the plane passing through the earth, perpendicular to the equatorial plane and containing the dawn-dusk axis). As shown in Fig. 1(c), Guo et al. (2010) and Li et al. (2012, 2013) also found two edges, which correspond to two modes of K-H waves propagating along these inner and outer edges.

However, none of these authors have linked with the important work of Kármán on structures named "Kármán vortex (KV) street" [*Von Karman*, 1963; 2004] (a detailed review can be found in [*Wille*, 1960]). Besides, their related significant physical processes on the vortex shedding, nondimensionalized shedding frequency "Strouhal number" [*Gruszecki et al.*, 2010; *Samanta et al.*, 2019], mechanism on converting from unstable transverse to stable longitudinal vortexes (Fig. 1(a)) [*A Hussain*, 1983; *A F Hussain*, 1986; *Kida*, 2006; *Kida and Miura*, 1998; *Kida and Yanase*, 1999], and the global magnetospheric coherent structure, etc. have never been discussed. As displayed in Fig. 2(a), it is well known that in the wake flow behind a cylinder-like object, a vortex train forms and aligns along two nearby separate lines. In the figure, the theoretical aspect ratio of the vortex spacings b/a is ~0.281. However, due to different wake flow conditions where the obstacles are not always a cylinder, the aspect ratios b/a may vary from approximately 0.28 to 0.52 [*Chopra and Hubert*, 1965].

In the present paper, we will refer to the vortex flow as KV street if the aspect ratio b/a are close to the range from approximately 0.28 to 0.52.

The KV streets in a plasma flow or magnetized medium have not been studied well. However, they are known to play key roles in numerous applications. For example, in industrial MHD, the effect of Alfvenic vortex shedding can be used for averaging the temperature by convective transport in liquid metals [*Dousset and Pothérat*, 2008]. In a controlled fusion, this effect is studied in association with the formation of coherent structures (blobs) in the scrape-off layer in tokamak plasmas [*Aydemir*, 2005].

The KV street is considered to be one of the key features to understand the coherent structures observed /expected in a turbulent free shear flow [*Holmes et al.*, 1998]. The main goals of the present study are to answer the following questions:

(i) Numerous satellite observations detect the regular shedding of K-H boundary waves/vortexes at/around the magnetopause. These vortexes are unstable and become to be turbulent in a single row. However, those numerous satellite observations do observe relatively stable regular vortex shedding like those of Kármán vortex street after a cylinder. This has long been the mystery.

(ii) The K-H instability is a linear instability and can generate transverse vortexes. The transverse vortexes are unstable and have to be converted to the stable longitudinal vortexes to be coherent. The longitudinal vortex is a vortex whose core line is approximately in the direction of the flow. In magnetospheric flow, it has been a question of how those transverse vortexes are converted to the stable longitudinal vortexes, how those longitudinal vortexes persist, survive, and constitute the global magnetospheric coherent structures.

Sections 2 and 3 summarize the main features of the so-called Karman Vortex (KV) street and Strouhal number in the 3D global MHD simulations, respectively, which are used herein. Section 4 presents the main results obtained herein in the view of KV street, Strouhal number, and the magnetospheric coherent structure, and the conclusions are provided in Section 5.

2, Kármán Vortex Street

2.1 Karman Vortex Street Review

In a complex plane of a potential flow, we define the complex velocity of potential *f(z)* of the flow around a single vortex as follows:

$$f(z) = \phi + i\psi = \frac{\Gamma}{2\pi}\theta - i\frac{\Gamma}{2\pi}\log r = \frac{\Gamma}{2\pi i}\log re^{i\theta} = \frac{\Gamma}{2\pi i}\log z, \qquad (1)$$

where the circulation $\Gamma = \int_0^{2\pi} v_\theta r\, d\theta = 2\pi r v_\theta$, the velocity potential $\phi = \frac{\Gamma}{2\pi}\theta$, the stream function $\psi = -\frac{\Gamma}{2\pi}\log r$, and $v_\theta = \frac{\partial\phi}{r\partial\theta} = -\frac{\partial\psi}{\partial r}$. The KH instability generates a single vortex sheet based on rows located at a distance "*a"* one from each other (Fig. 2(a)). This vortex sheet can be expressed by summing all *2n+1* complex velocity potentials of Eq. (1), taking $n \to \infty$, we obtain $f(z) = \frac{\Gamma}{2\pi i}\log\left(z\ \sin\frac{\pi z}{a}\right)$. However, this single line vortex sheet is unstable. To model a "stable" linear staggered point vortex sheets as shown in Fig. 2(a) on which one adds small disturbances x^0. The complex velocity potential associated with this double vortex sheet can be expressed as:

$$f(z) = \frac{\Gamma}{2\pi i}\log z\ \sin\frac{\pi}{a}\left(z - \frac{ib}{2}\right) - \frac{\Gamma}{2\pi i}\log z\ \sin\frac{\pi}{a}\left(z - x^0 + \frac{ib}{2}\right). \qquad (2)$$

It is known that, in the double vortex sheets defined for a static flow, the motion of a single vortex is entirely induced by all other vortex velocities [*Wille*, 1960]. Obtaining the induced velocity of the single vortex, we get the neutral (marginal) stability condition of the vortexes as follows:

$$R = \frac{b}{a} \sim 0.28, \qquad (3)$$

where *R*, *a*, and *b* are, respectively, the aspect ratio of the vortexes, distance between vortex cores along and perpendicular to the direction of the vortex alignment (which is also the direction of the main flow) as illustrated in Fig. 2(a). We call this vortex alignment Karman Vortex (KV) Street. In the present paper, we will refer to the vortex flow as KV street if the aspect ratio b/a are close to this value.

Quantitative comparison between this theory and 3D global MHD numerical simulation obtained for north IMF result is performed as follows:

Figure 1(b) represents 2D cut of velocity vectors $(\mathbf{V} - \mathbf{U})$ in the equatorial plane from the 3D global MHD simulation from [*Merkin et al.*, 2013], where $\mathbf{V}$ is the local velocity, and $\mathbf{U}$ is the uniform flow. If we focus on two rows of vortexes, we obtain $R \sim 0.28$.

Figure 1(c) represents a 2D cut of the velocity V_x contour in the equatorial

plane from the 3D global MHD simulation of [*Guo et al.*, 2010; *Li et al.*, 2013]. If we focus on two rows of vortices, we obtain $R = b/a \sim 0.29$.

Figure 1(d) represents the equatorial slice viewing from the z-direction with both V_x isocolors and velocity vectors from our 3D global MHD simulations [*Kubota et al.*, 2015]. Here, we obtain $R \sim 0.28$. The white vectors are the 3D flow vectors starting on the equatorial plane. The black and white dots, respectively, indicate the vortex cores or Galilean invariants along the outer and inner edges within the equatorial plane. They are aligned as KV street. The vortexes start from about θ_{sh} ~20°-30° from the subsolar line. The blue lines indicate the way R=b/a is measured.

All these three estimates from the 3D global simulations suggest that, after the K-H vortexes roll-up in the dayside, the curvature effects of the magnetopause shed these vortices off this frontier, and a secondary flow forms the so-called Alfvenic KV street at/around the magnetopause. This is more evident near the dawn-dusk "terminator."

2.2 Generation Mechanisms and Reynolds number

Figure 3 shows our simulation results of KV street at/around the subsolar point. Black and white dots are the cores of vortexes obtained by the method described in [*Cai et al.*, 2018]. In both dusk and dawn sides, the two staggered lines of vortices are generated and move tailward with the vortex-induced speed mentioned in section 2.1. These vortices are broken-down by nonlinear instabilities [*A Hussain*, 1983; *A F Hussain*, 1986; *Kida*, 2006; *Kida and Miura*, 1998; *Kida and Yanase*, 1999] in the night side at/around x~-20 to -30 Re behind the dawn-dusk "terminator" as shown in Fig. 4.

The mechanism responsible for the generation of the internal vortexes is still unknown. However, we have a large stagnation flow region (i. e., the region with no positive shear flow) illustrated by a large green area and limited by a thick dashed black line in Fig. 3. The unknown periodic large wake flows from the earth to the sun hit this region, and these flows are inflected and make almost 90° turns tailward in both the dawn and dusk sides, as illustrated by the two thick black arrows and the yellow islands that are positive v_x areas in Fig. 3 (a). The positive shear flows v_θ are indicated by the yellow islands in the dusk side and the blue islands in the dawn side in Fig. 3(b). The origin of this wake flow is unclear and still under investigation. These two inflected flows generate the different shears within the magnetosphere (inside) from those within

157 the magnetosheath (outside). Both shears inside and outside the magnetopause are at the
158 origin of the "KV streets."
159 In fluids dynamics or MHD, the Reynolds number (R_E) is a dimensionless
160 quantity defined as the ratio of momentum forces to viscous forces $R_E = UL/\nu$, where
161 U is the uniform flow velocity relative to the object (here the magnetosphere), L is the
162 characteristic linear dimension that is the length of the flow travels (here the length of
163 the stagnant region in Fig. 3), and ν is the kinematic viscosity.. This number is often
164 used to classify similar flow patterns in different flow conditions as illustrated in Fig.
165 2(b) [*Blevins*, 1977]. The Reynolds number of the magnetosphere can be estimated
166 using the kinematic viscosity of the plasma flow, $\nu = v_i^2/2\Omega_i = v_i r_i/2$, as proposed by
167 Hultqvist [*Hultqvist*, 1999], where $v_i = \sqrt{\frac{T_i}{M_i}}$ is the ion thermal velocity, $r_i = v_i/\Omega_i$ is
168 the ion gyro-radius, Ω_i is the ion gyro-frequency, M_i is the ion mass, and T_i is the
169 ion temperature. In the present case, using parameters in [*Kubota et al.*, 2015] and the
170 obtained characteristic linear dimension L that is the size of the indicated stagnant area
171 (the minor axis length of the ellipse in Fig. 3, with a size roughly 2-4 earth radii (R_e),
172 indicated by dashed thick curves near subsolar point), the estimated Reynolds number in
173 the present paper is R_E~ 106-212. According to the classification of Fig. 2(b), the
174 estimated value is high enough so that one can expect that the plasma flow patterns
175 at/around the magnetopause and at the wake of the magnetosphere are in the regime of
176 "Kármán vortex (KV) street" as illustrated in the rectangle of Fig. 2(b).
177
178 2.3 Strouhal Number
179 The periodic generation of Alfvenic vortexes is one of the most significant
180 characteristics of KV street. The Strouhal number (St) is a dimensionless number
181 describing the frequency of the vortex shedding, which is also the frequency of the flow
182 oscillation behind the obstacle [*White*, 1999]. The Strouhal number is commonly
183 defined as $St = f\frac{L}{U}$, where f is the frequency of vortex occurrence, L is the
184 characteristic linear dimension, and U is the uniform flow velocity. Figure 2(c) shows
185 the variation of the Strouhal number versus the Reynolds number in the example of a
186 long cylinder, as Reynolds number varies from the orders of 10^1 to 10^7. The value of
187 Strouhal number is characterized by the buildup of vortexes with a repeated occurrence

frequency behind a long cylinder. It ranges from 0.12 to 0.2 as the Reynolds number varies from 40 to 250 [*White*, 1999], and remains around 0.2 for the larger Reynolds number ($250 < Re < 10^5$). Let us precise that the two curves of Figure 2(c) are obtained for different types of cylinder surfaces and differ one each other for $Re > 10^5$ (out of interest in the present study).

In the present 3D MHD simulation, the solar wind velocity is U=835km/s, the measured vortex occurrence frequency is f=0.0087. Thus, using typical characteristic linear dimensions L~2.6, we can estimate the Strouhal number value St~0.17, which roughly coincides with the Strouhal number range (black rectangle) indicated in Figure 2(c) for a cylinder model. This agreement suggests that the stagnant area defined within the magnetosphere can be considered as a cylindrical obstacle behind which stable longitudinal vortex structures are generated.

3, Magnetospheric Coherent structures

In the previous section, we have discussed the shed KV vortexes are transverse (i. e., core lines are transverse to the flow and thus are unstable to the flow). The regions around the vortex-cores defined from the three different 3D MHD global simulations in Figs. 1(b-d), and black/white dots in Fig. 3 evidence the formation of the KV streets on the equatorial plane since the Karman aspect ratio is all about 0.28. This KV street continues until x~ -10 to -20 Re, and nonlinear instabilities destroy the structure of these transverse vortexes as shown in Fig. 4.

Figure 4(a) shows the schematic view of the magnetospheric coherent structures at the equatorial plane, and Fig. 4(b) shows its related 3D vortex core lines projected onto the equatorial or XY plane from +z direction in our 3D global MHD simulations. In the dayside region near the subsolar point, the K-H vortexes develop along the 3D magnetopause surface, and, thus, their vortex core lines start from both near north and south poles to the equatorial plane along the magnetopause surface radially. Observing from the development of vortex core lines in Fig. 4(b), the vortexes start from the radial unstable transverse features, are converted to the stable longitudinal vortexes in the night side, and these longitudinal vortexes survive for long time until x~-130 to -140 Re and constitute the global magnetospheric coherent structures. In Fig. 4, whole magnetospheric coherent turbulent dynamics can be inspired both from the previous turbulence works [*A Hussain*, 1983; *A F Hussain*,

1986; *Kida*, 2006; *Kida and Miura*, 1998; *Kida and Yanase*, 1999; *Miura and Kida*, 1997; *Moffatt et al.*, 1994] and deduced from our 3D MHD simulations, and this allows us to identify 5 regions in the simulations as follows:

1. Region I K-H vortexes: The K-H vortexes where their vortex-core-lines are transverse to the flow grow linearly in the shear layers from the subsolar point and shifted to about θ_{sh} ~ 20-30° from the x-axis tailward on the equatorial plane. They are generated along inside and outside magnetopause surfaces and extend radially from the polar regions to equator planes along the magnetopause surface. Thus, they have 3D arc structures.
2. Region II Vortex Shedding: After θ_{sh} ~ 20-30° from the x-axis tailward, the developed vortexes by K-H instability shed off from the shear layer.
3. Region III KV streets: The transverse vortexes move freely approaching the marginal stable configuration forming staggered two-vortex rows (i.e., KV street shown in Fig. 2(a)) inside/outside the velocity shear region across the magnetopause. The KV streets continue from x~-10 to -20 Re.
4. Region IV Vortex Break-down: The Karman transverse vortex sets near the equatorial plane soon become unstable due to 3D nonlinear effects. The so-called break-down of the transverse vortex occurs. They are the wavy dashed-lines in Region IV of Fig. 4(a)[*Kida*, 2006; *Kida and Miura*, 1998; *Kida and Yanase*, 1999; *Moffatt et al.*, 1994]; and
5. Region V Longitudinal (Stream-wise) vortexes: Finally, those scraped vortex-cores reconnect and reform into the stable longitudinal or stream-wise vortices after x~-20 to -30 Re and survive over a long time-period until x~-130 to -140 Re. These long survived stable vortexes may constitute to larger energy and momentum transports between the solar wind and magnetosphere than those by simple K-H instability in the dayside region.

These entire processes from Regions I to V lead to the "magnetospheric coherent structures" (for example see [*Hall*, 1972]). In these magnetospheric coherent structures, the complicated 3D wake flow mechanism to generate the Karman vortex street and to determine the nondimensionalized vortex shedding rate (Strouhal number) is one of the most important key factors to characterize the whole complex magnetospheric coherent structures.

4, Conclusions

Magnetopause in dayside near the subsolar point is a typical frontier where the well-known K-H instability is expected to develop linear vortexes. However, very few researchers have investigated the 3D structures and the behaviors of those shed vortexes. Many satellite observations claim that they observed and encountered a series of relatively regular K-H boundary waves. However, these vortexes induce each other by the mechanism discussed in section 2.1 and are unstable in one row. Thus, such satellite observations of the regular patterns of "K-H vortexes" have been a mystery for a while. In the present study, the structure and dynamics of the magnetopause are analyzed in terms of (i) KV street, (ii) Reynolds and Strouhal numbers, and (iii) 3D vortex build-up. These three approaches are complementary and shed some lights on the global view of the magnetopause properties with respect to previous works, in particular, to investigate the basic global process supporting the mass/momentum/energy transfers from the solar wind to the magnetosphere based on the concept of coherent structures concept.

Our main preliminary results obtained from recent three-dimensional global MHD simulations for the northward IMF configuration are summarized as follows:

(i) We show that a large stagnant flow region (L~2-4 Re) can be identified near the subsolar point. Along with inside and outside the magnetopause surfaces, two velocity shears which generate K-H vortexes with the opposite sign are generated, respectively, between (1) outside magnetopause and the solar wind, and (2) inside magnetopause and magnetospheric wake flows, behind the large stagnation flow region.

(ii) After θ_{sh} ~ 20-30°, the 3D arc-shaped vortexes shed off from the magnetopause shear layers, become 3D vortexes, induce each other, adjust themselves to form the so-called the KV street.

(iii) We show that the aspect ratio of two vortex distances both in a row and in a column is R=a/b~0.28 in KV street in three different MHD simulation.

(iv) We also show that the dimensionless Strouhal number is the order of St~0.17.

(v) Free transverse Karman vortexes can survive in the night side over a distance of x~-10 to -20Re.

(vi) After these transverse vortexes break-down, these soon reform into coherent longitudinal (stable) vortexes that survive over much longer distance x~-130 -

-140 Re in the night side.

In summary, the entire processes listed from *(i)* to *(vi)* constitute the magnetospheric coherent structures. Besides, we show that the dimensionless Strouhal number is very close to the value we measure on the ground fluid experiment as shown in Fig. 2(c).

This magnetospheric coherent structure should be more intensively analyzed using recent high resolution large-scale global simulations. Besides, these different vortexes should be able to be observed and identified in the tetrahedrally-configured satellite sets such as Cluster and MMS mission.

Acknowledgment

We would like to thank the Research Institute of Sustainable Humanosphere for providing access to Advanced Kyoto-Daigaku Denpa-Kagaku Keisanki-Jikken (A-KDK) supercomputers. We would like to thank valuable comments from Dr. Takashi Tanaka. The 3D Global MHD simulation data used in the present paper are deposited at Zendo (DOI:10.5281/ zenodo.3951048)

References

Aydemir, A. (2005), Convective transport in the scrape-off layer of tokamaks, *Physics of plasmas*, *12*(6), 062503.

Blevins, R. D. (1977), *Flow-induced vibration*, 377 pp., Van Nostrand Reinhold Co., New York.

Cai, D., B. Lembege, H. Hasegawa, and K. I. Nishikawa (2018), Identifying 3-D Vortex Structures At/Around the Magnetopause Using a Tetrahedral Satellite Configuration, *Journal of Geophysical Research-Space Physics*, *123*(12), 10158-10176, doi:10.1029/2018ja025547.

Chandrasekhar, S. (1968), *Hydrodynamic and hydromagnetic stability*, Clarendon Press.

Chopra, K., and L. Hubert (1965), Mesoscale eddies in wake of islands, *Journal of the Atmospheric Sciences*, *22*(6), 652-657.

Dousset, V., and A. Pothérat (2008), Numerical simulations of a cylinder wake under a strong axial magnetic field, *Physics of Fluids*, *20*(1), 017104.

320 Gruszecki, M., V. M. Nakariakov, T. Van Doorsselaere, and T. Arber (2010),
321 Phenomenon of Alfvénic vortex shedding, *Physical review letters*, *105*(5),
322 055004.
323 Guo, X., C. Wang, and Y. Hu (2010), Global MHD simulation of the
324 Kelvin-Helmholtz instability at the magnetopause for northward
325 interplanetary magnetic field, *Journal of Geophysical Research: Space*
326 *Physics (1978-2012)*, *115*(A10).
327 Hall, M. (1972), Vortex breakdown, *Annual Review of Fluid Mechanics*, *4*(1),
328 195-218.
329 Holmes, P., J. L. Lumley, and G. Berkooz (1998), *Turbulence, coherent*
330 *structures, dynamical systems and symmetry*, Cambridge university press.
331 Hultqvist, B. (1999), *Magnetospheric plasma sources and losses: Final report*
332 *of the ISSI study project on source and loss processes of magnetospheric*
333 *plasma*, Springer Science & Business Media.
334 Hussain, A. (1983), Coherent structures reality and myth, *Physics of Fluids*
335 *(1958-1988)*, *26*(10), 2816-2850.
336 Hussain, A. F. (1986), Coherent structures and turbulence, *Journal of Fluid*
337 *Mechanics*, *173*, 303-356.
338 Kida, S. (2006), *IUTAM Symposium on Elementary Vortices and Coherent*
339 *Structures: Significance in Turbulence Dynamics: Proceedings of the IUTAM*
340 *Symposium held at Kyoto International Community House, Kyoto, Japan,*
341 *26-28 October, 2004*, Springer Science & Business Media.
342 Kida, S., and H. Miura (1998), Identification and analysis of vortical
343 structures, *European Journal of Mechanics-B/Fluids*, *17*(4), 471-488.
344 Kida, S., and S. Yanase (1999), *Turbulent Flow Dynamics*, Asakura Pub.,
345 Tokyo.
346 Kubota, Y., R. Kataoka, M. Den, T. Tanaka, T. Nagatsuma, and S. Fujita
347 (2015), Global MHD simulation of magnetospheric response of preliminary
348 impulse to large and sudden enhancement of the solar wind dynamic
349 pressure, *Earth, Planets and Space*, *67*(1), 94,
350 doi:10.1186/s40623-015-0270-7.
351 Li, W., X. Guo, and C. Wang (2012), Spatial distribution of Kelvin -

352 Helmholtz instability at low - latitude boundary layer under different solar
353 wind speed conditions, *Journal of Geophysical Research: Space Physics*,
354 *117*(A8).
355 Li, W., C. Wang, B. Tang, X. Guo, and D. Lin (2013), Global features of
356 Kelvin-Helmholtz waves at the magnetopause for northward interplanetary
357 magnetic field, *Journal of Geophysical Research: Space Physics*, *118*(8),
358 5118-5126.
359 Merkin, V., J. Lyon, and S. Claudepierre (2013), Kelvin-Helmholtz instability
360 of the magnetospheric boundary in a three-dimensional global MHD
361 simulation during northward IMF conditions, *Journal of Geophysical*
362 *Research: Space Physics*, *118*(9), 5478-5496.
363 Miura, H., and S. Kida (1997), Identification of tubular vortices in turbulence,
364 *Journal of the Physical Society of Japan*, *66*(5), 1331-1334.
365 Moffatt, H., S. Kida, and K. Ohkitani (1994), Stretched vortices: the sinews
366 of turbulence; large-Reynolds-number asymptotics, *Journal of Fluid*
367 *Mechanics*, *259*, 241-264.
368 Samanta, T., H. Tian, and V. M. Nakariakov (2019), Evidence for Vortex
369 Shedding in the Sun's Hot Corona, *Physical review letters*, *123*(3), 035102.
370 Santos, M., A. Coutinho, and M. Schubert Pfeil (2017), *Vortex Shedding by*
371 *LES 3D Numerical Simulation*, doi:10.20906/CPS/CILAMCE2017-0785.
372 Von Karman, T. (1963), *Aerodynamics*, Cornell University press: Mc
373 Graw-Hill company.
374 Von Karman, T. (2004), *Aerodynamics: selected topics in the light of their*
375 *historical development*, Courier Corporation.
376 White, F. M. J. E. M.-H. B. (1999), Fluid mechanics, WCB.
377 Wille, R. (1960), Karman vortex streets, *Advances in Applied Mechanics*, *6*,
378 273-287.
379

380 **Figure Caption**

381 Figure 1: (a) Schematic views of a transverse (left) and a longitudinal vortex (right). (b)
382 2D cut of the velocity vector plot ($\delta\mathbf{v} = \mathbf{V}\text{-}\mathbf{U}$) at the equatorial plane from the 3D global
383 MHD simulation (Fig. 6 (a) from [*Merkin et al.*, 2013]), where $\mathbf{V}$ is the local velocity,
384 and $\mathbf{U}$ is the uniform flow. (c) 2D cut of the velocity V_x iso-contours in the equatorial

plane from the 3D global MHD simulation ([*Guo et al.*, 2010; *Li et al.*, 2013]). (d) Equatorial slice viewing from the +z-direction with both V_x isocolors and velocity vectors.

Figure 2: (a) Schematic diagram of the KV street. (b) Sketches of Reynolds number regimes for different typical flow patterns across a cylinder: (i) Regime of unseparated flow; (ii) A fixed pair of vortices in wake; (iii)Two regimes where a vortex street is laminar; (iv)Two regimes where the flow transits to turbulence in vortex, and vortex street is fully turbulent; (v) Laminar boundary layer has undergone turbulent transition and wake is narrower and unorganized; and (vi) Re-establishment of the turbulent vortex street [*Blevins*, 1977]. The rectangle corresponds to the possible flow regime for magnetospheric condition discussed herein. (c) Relationship between Reynolds number R_E and Strouhal number St, obtained from experimental models of cylinders in two-dimensions flow conditions (reproduced from [*Santos et al.*, 2017]). The rectangle corresponds to the magnetospheric flow regime, where the arrow indicates St~0.17.

Figure 3: The figure is the same as Fig. 1(d) with a wider view near the subsolar point. The 2D plot of the equatorial plane with both the (a) V_x and (b) V_θ contour colors, and velocity vectors. The black and white dots indicate the vortex cores in the outer and inner edges on the equatorial plane, respectively.

Figure 4: (a) Schematic view of five steps or regions illustrating the coherent vortex developments and coherent structures (Regions I to V) within the equatorial plane (X-Y). The dashed wavy lines in the magnetotail indicate the occurrence of the vortex breakdown. (b) Top view from the +z-direction and 3D projection of vortex core-lines (black zigzag line) onto the XY or the equatorial plane.

Figure1.

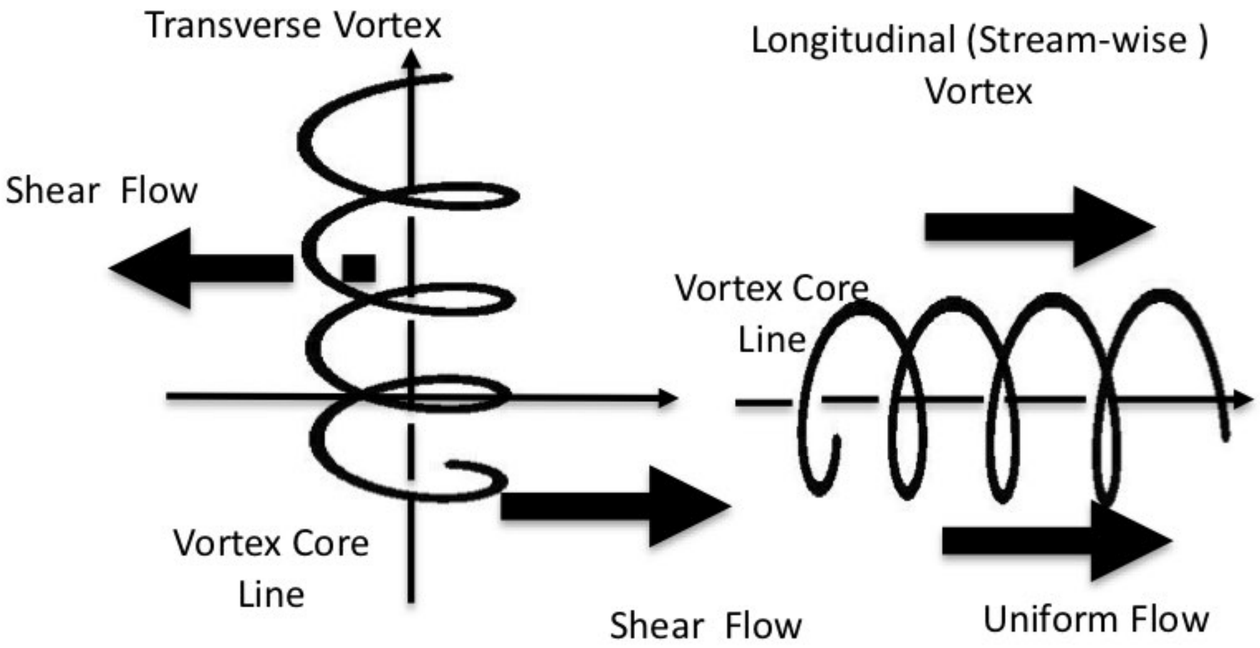
Transverse Vortex
Longitudinal (Stream-wise) Vortex
Shear Flow
Vortex Core Line
Vortex Core Line
Shear Flow
Uniform Flow

(a)

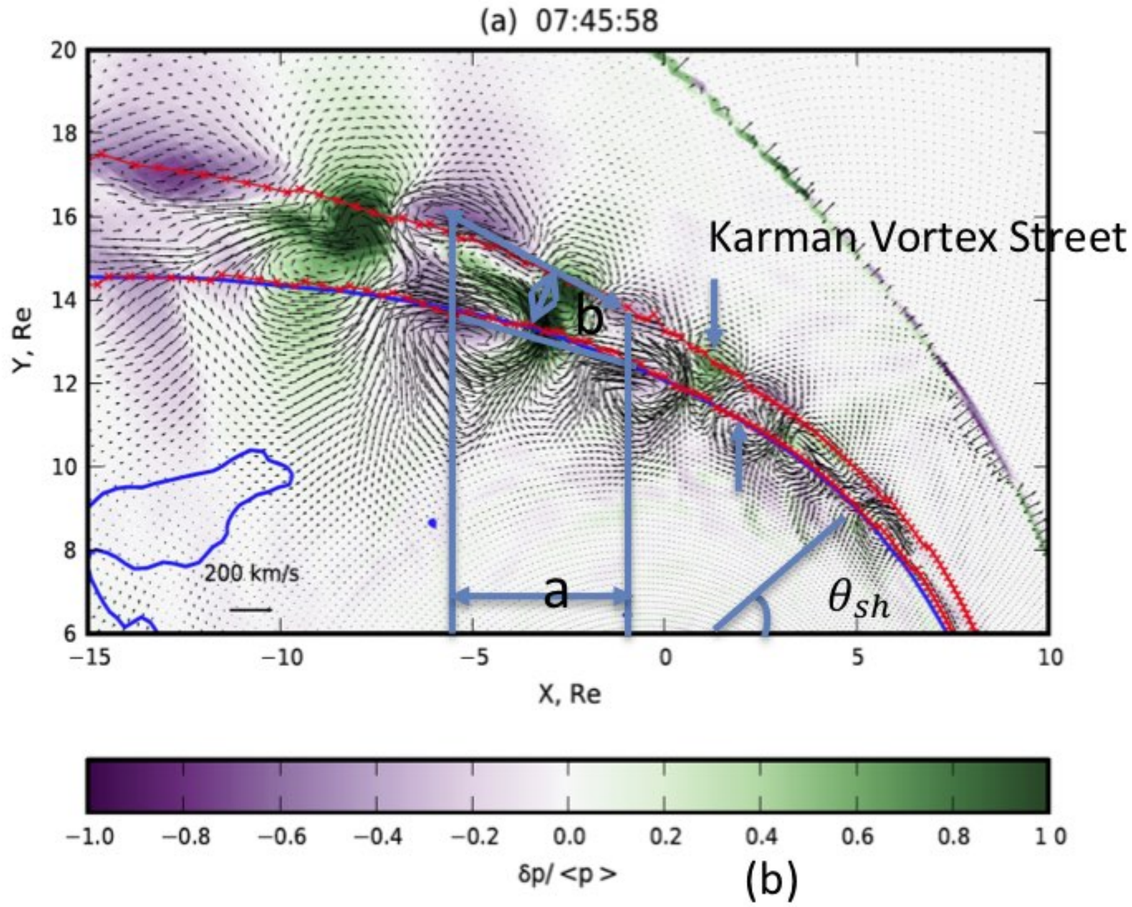
(a) 07:45:58
Karman Vortex Street
b
a
θ_{sh}
200 km/s
Y, Re
X, Re
δp/ <p >
(b)

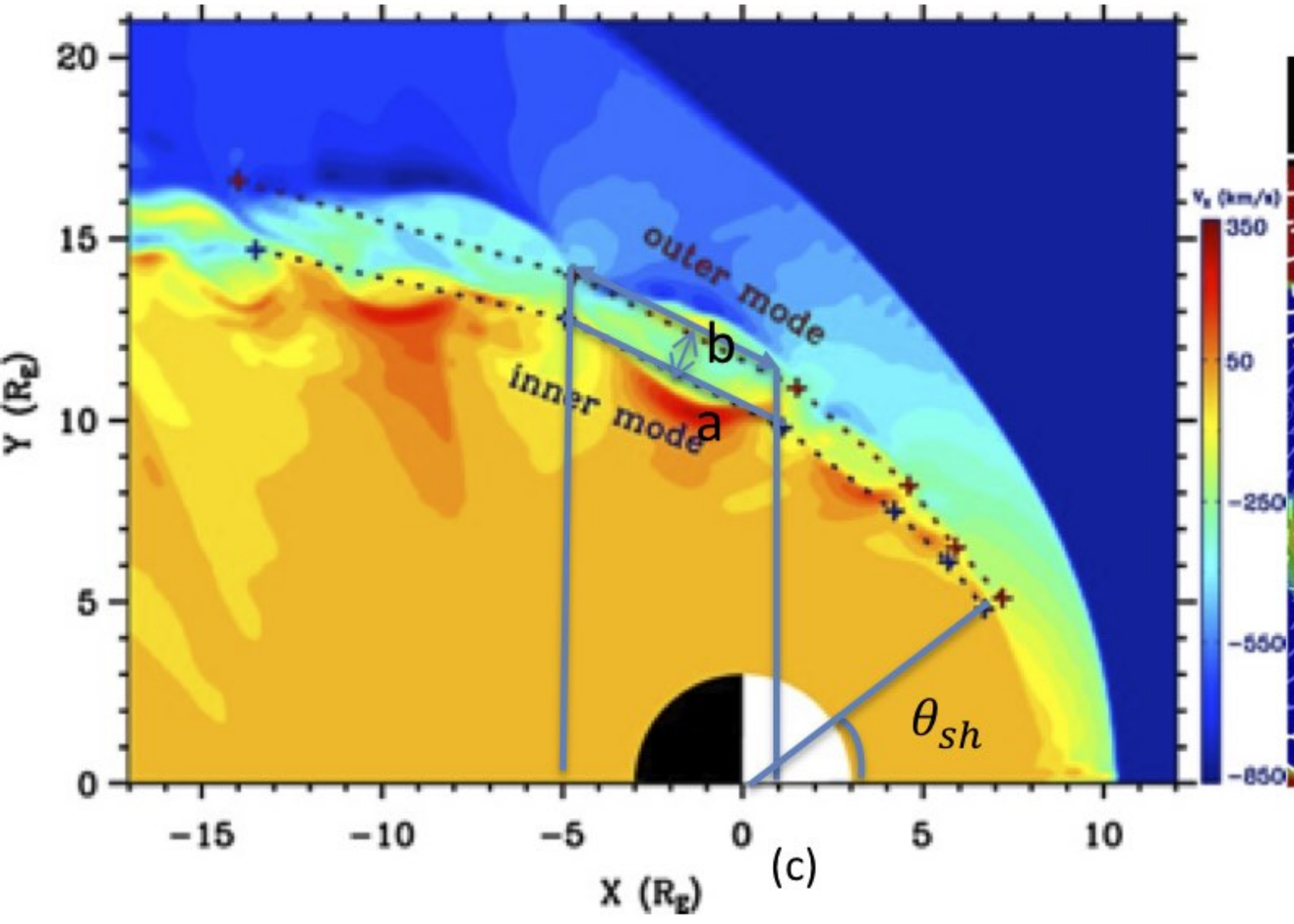
outer mode
inner mode
b
a
θ_{sh}
Y (R$_E$)
X (R$_E$)
(c)

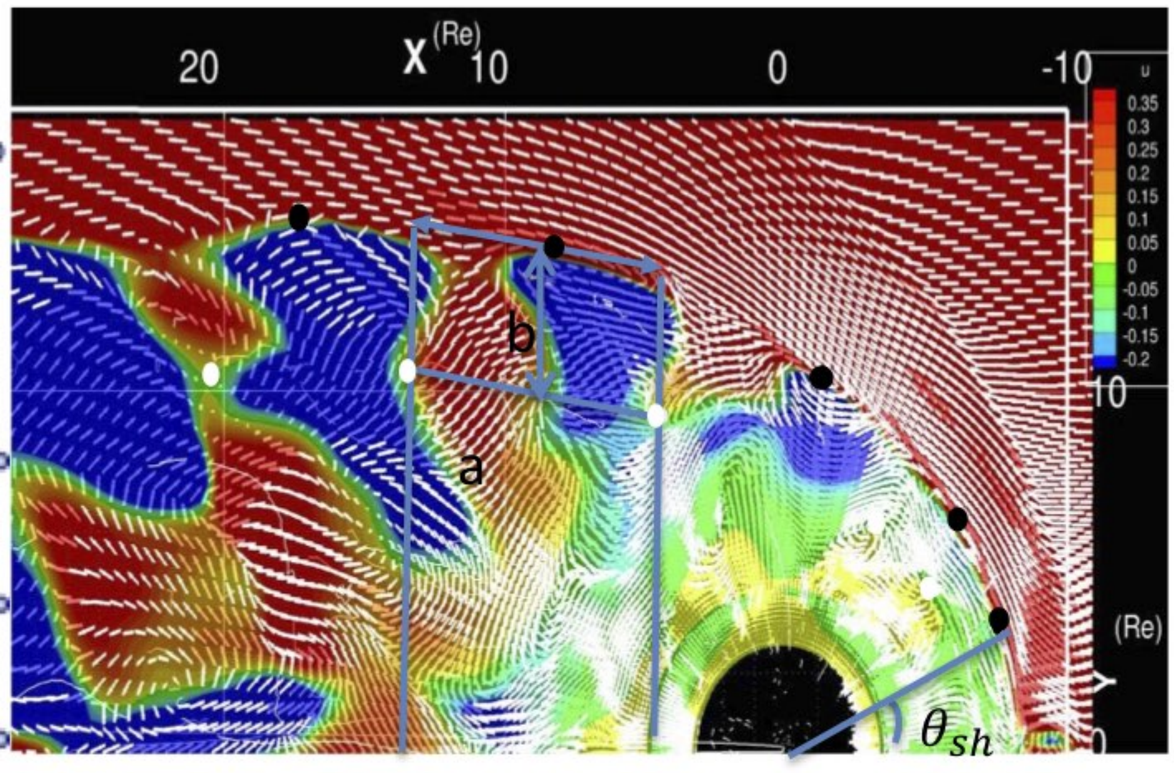
X (Re)
b
a
θ_{sh}
(Re)
(d)

Figure2.

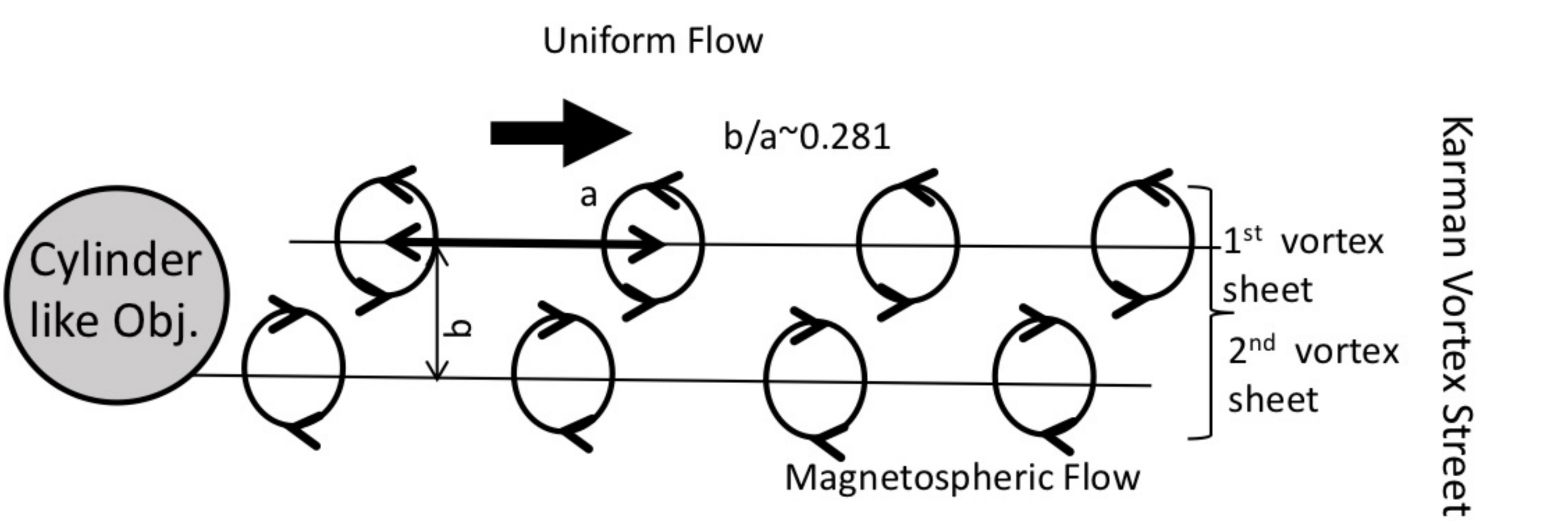
Uniform Flow
b/a~0.281
a
b
Cylinder like Obj.
1st vortex sheet
2nd vortex sheet
Magnetospheric Flow
Karman Vortex Street

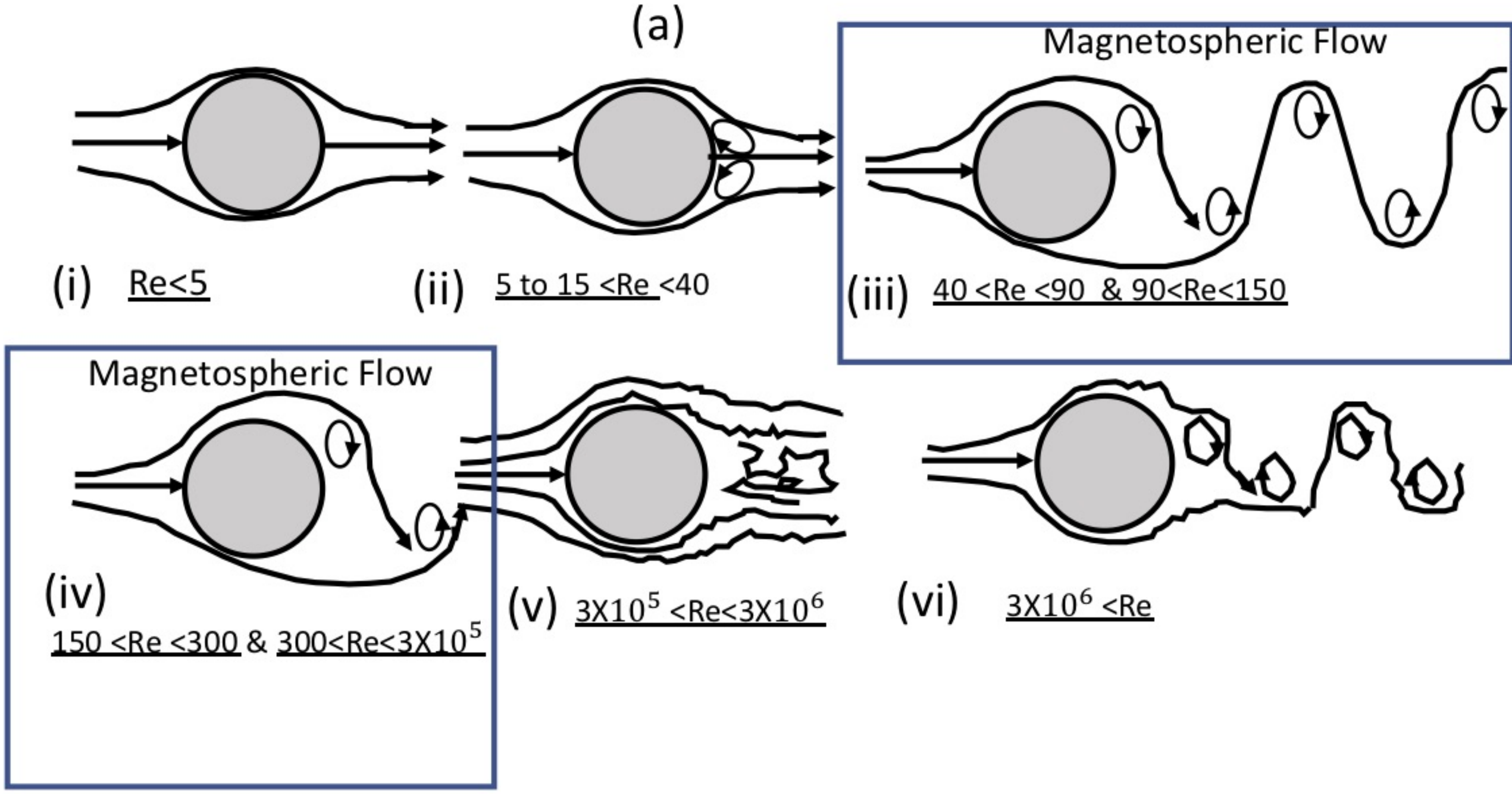
(a)
Magnetospheric Flow
(i) Re<5
(ii) 5 to 15 <Re <40
(iii) 40 <Re <90 & 90<Re<150
Magnetospheric Flow
(iv)
150 <Re <300 & 300<Re<3X10^5
(v) 3X10^5 <Re<3X10^6
(vi) 3X10^6 <Re

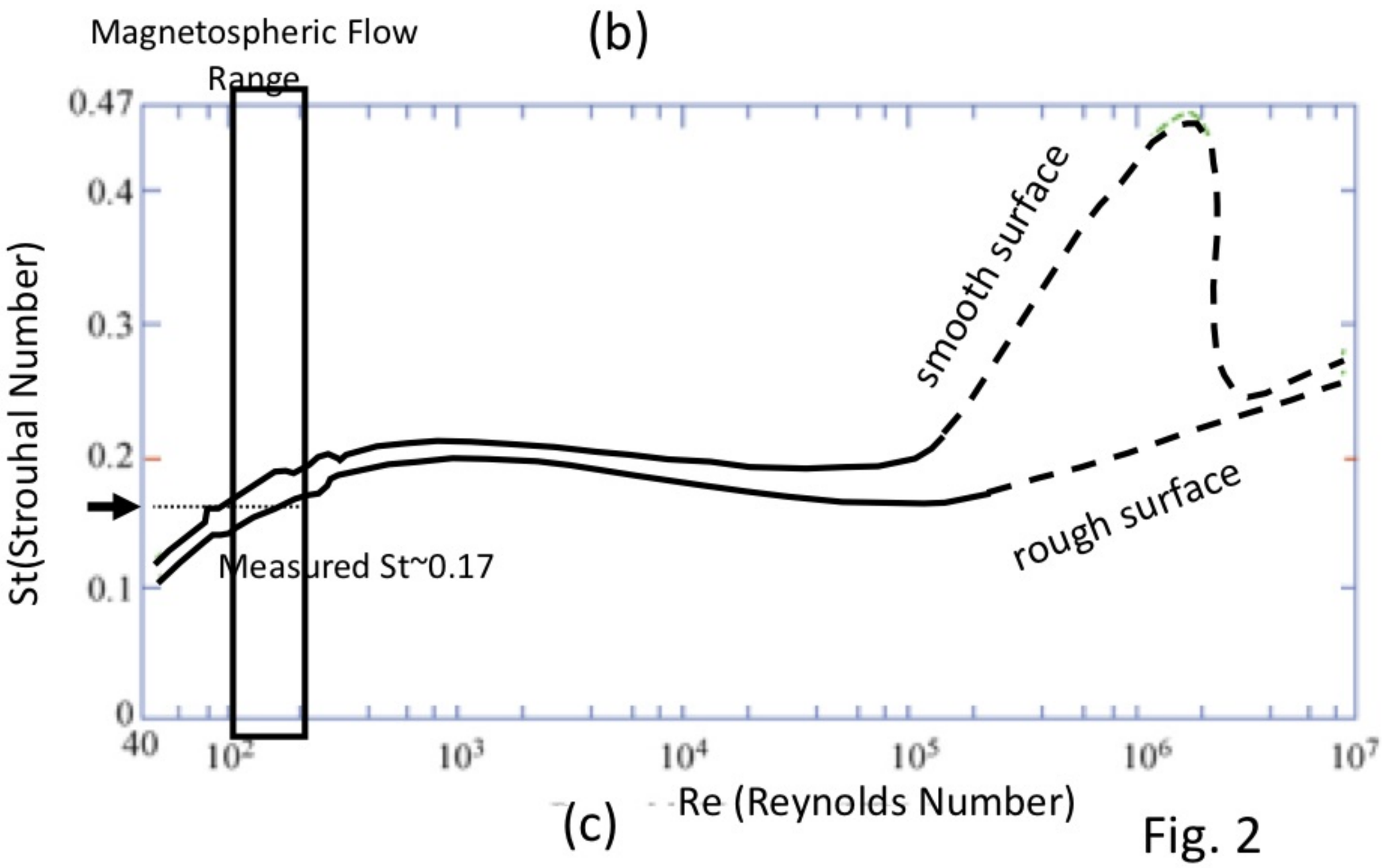
(b)
Magnetospheric Flow Range
St(Strouhal Number)
Re (Reynolds Number)
smooth surface
rough surface
Measured St~0.17
0.47
0.4
0.3
0.2
0.1
0
40
10^2
10^3
10^4
10^5
10^6
10^7

(c)

Fig. 2

Figure3.

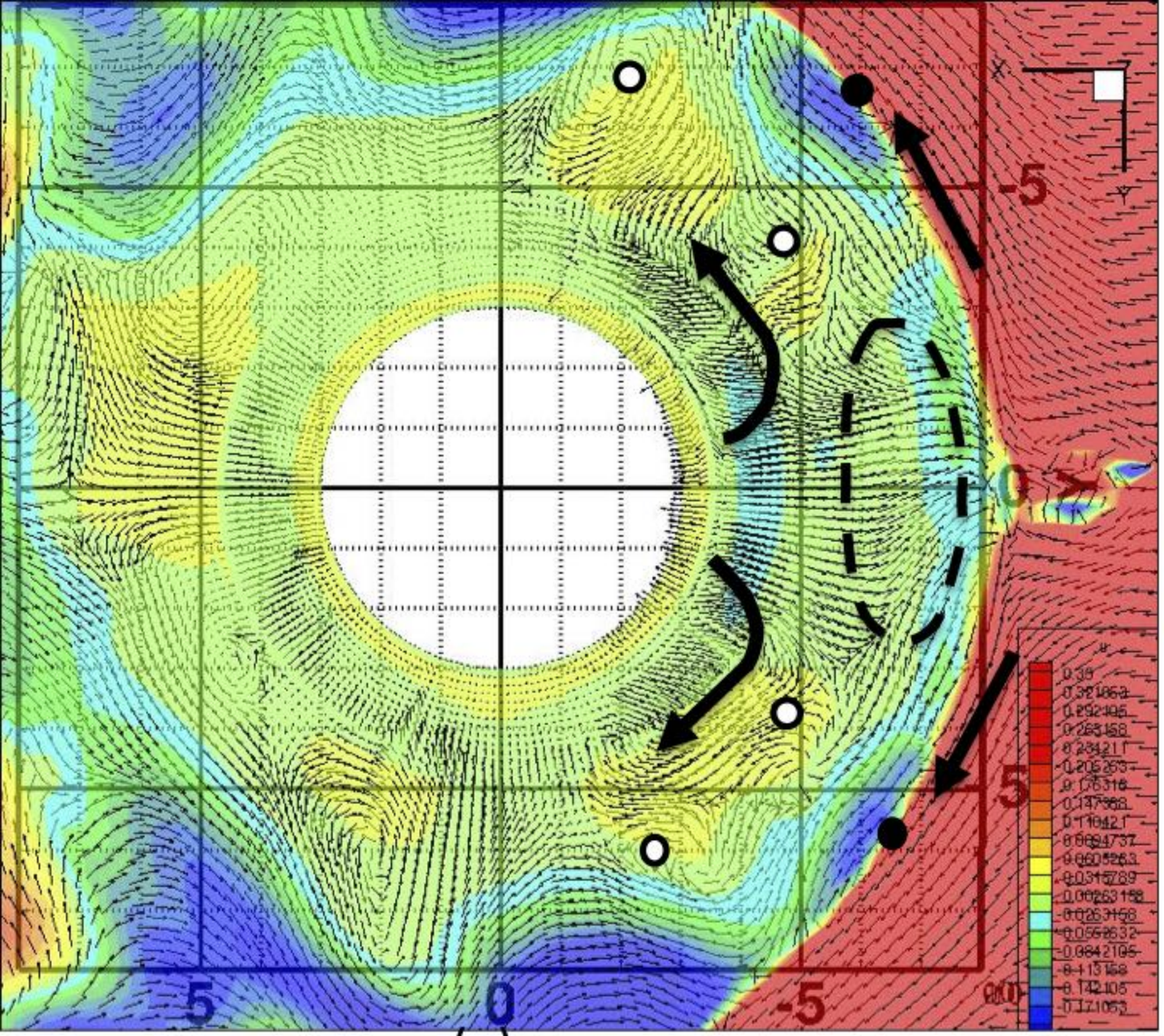

(a)

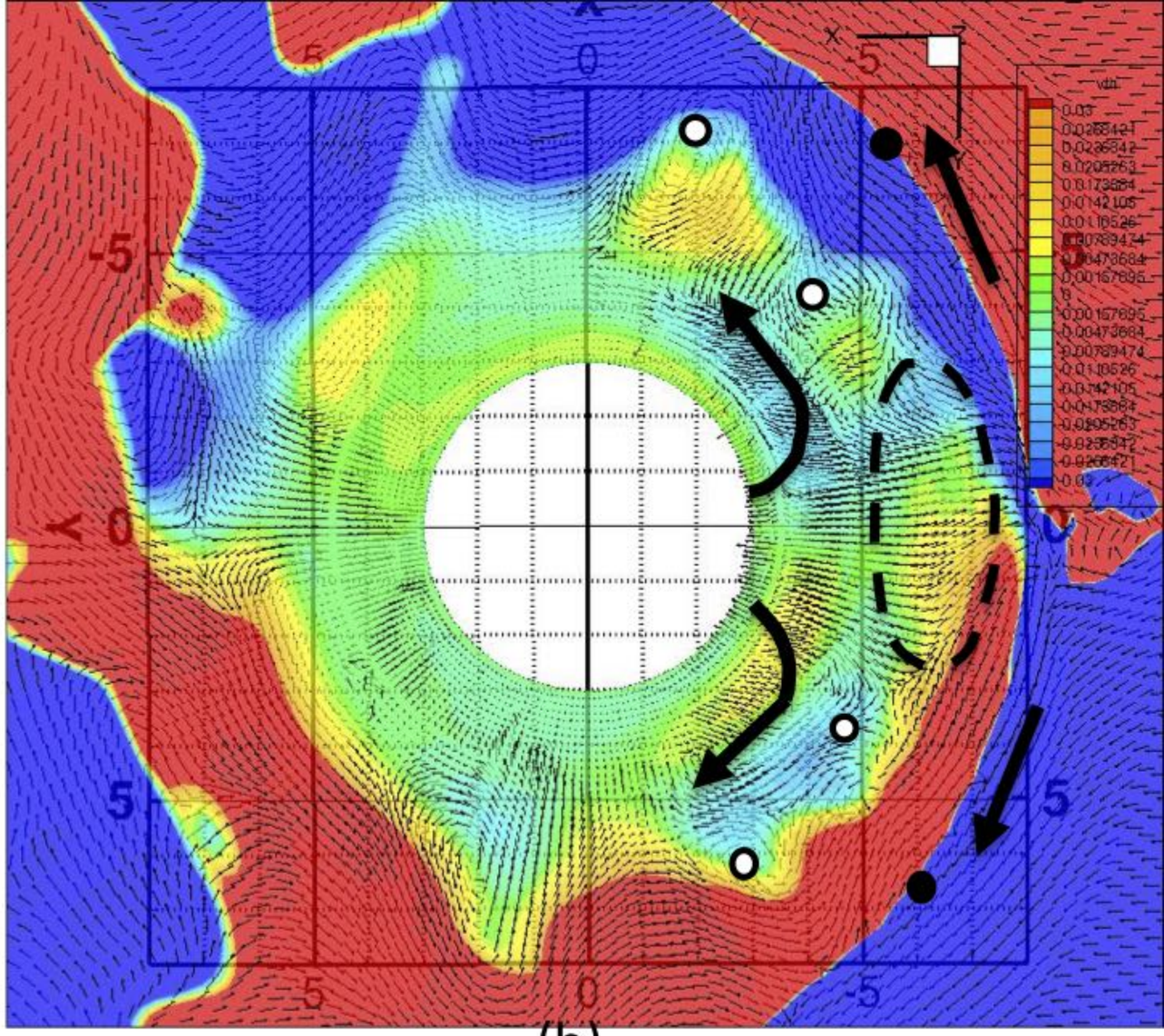

(b)

Figure4.

Longitudinal (Stream-wise) Vortex Core Lines

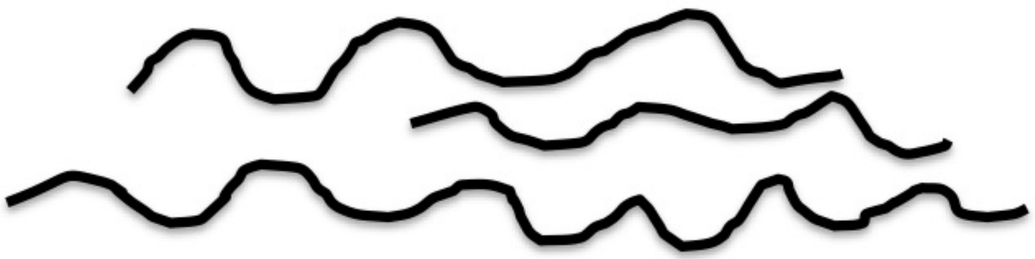

DD line

IMF B

Magnetopause

Solar Wind

Turbulent Flow

Turbulent Flow

Wake Flow

Stagnant flow

Y

X

Z

KH vortices

Region V: Stream-wise Vortices

Region IV: Vortex Break-down

Region III: Karman Vortex Street

Region II: Vortex Shedding

Region I:

Magnetotail region

Dayside region